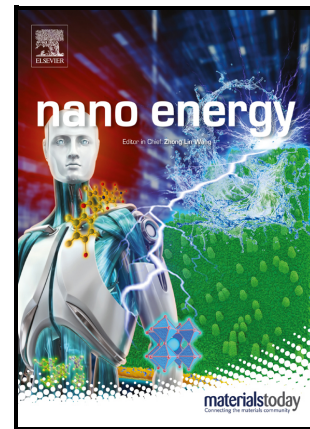


Triboelectric–electromagnetic hybridized module for energy harvesting of power transmission lines galloping and self-powered galloping state monitoring

Sihang Gao, Xisong Zeng, Guowen Zhang, Jiajia Zhang, Yiduo Chen, Shaoxuan Feng, Wenyu Lan, Jie Zhou, Zhong Lin Wang



PII: S2211-2855(22)00607-3

DOI: <https://doi.org/10.1016/j.nanoen.2022.107530>

Reference: NANOEN107530

To appear in: *Nano Energy*

Received date: 30 April 2022

Revised date: 10 June 2022

Accepted date: 21 June 2022

Please cite this article as: Sihang Gao, Xisong Zeng, Guowen Zhang, Jiajia Zhang, Yiduo Chen, Shaoxuan Feng, Wenyu Lan, Jie Zhou and Zhong Lin Wang, Triboelectric–electromagnetic hybridized module for energy harvesting of power transmission lines galloping and self-powered galloping state monitoring, *Nano Energy*, (2022) doi:<https://doi.org/10.1016/j.nanoen.2022.107530>

This is a PDF file of an article that has undergone enhancements after acceptance, such as the addition of a cover page and metadata, and formatting for readability, but it is not yet the definitive version of record. This version will undergo additional copyediting, typesetting and review before it is published in its final form, but we are providing this version to give early visibility of the article. Please note that, during the production process, errors may be discovered which could affect the content, and all legal disclaimers that apply to the journal pertain.

© 2022 Published by Elsevier.

# **Triboelectric–electromagnetic hybridized module for energy harvesting of power transmission lines galloping and self-powered galloping state monitoring**

Sihang Gao<sup>a, 1, \*</sup>, Xisong Zeng<sup>a, 1</sup>, Guowen Zhang<sup>a</sup>, Jiajia Zhang<sup>a</sup>, Yiduo Chen<sup>a</sup>, Shaoxuan Feng<sup>a</sup>,

Wenyu Lan<sup>a</sup>, Jie Zhou<sup>a</sup>, Zhong Lin Wang<sup>b, c, d, \*\*</sup>

<sup>a</sup> Key Laboratory of Industrial Internet of Things and Networked Control, Ministry of Education, Chongqing University of Posts and Telecommunications, Chongqing, 400065, China

<sup>b</sup> Beijing Institute of Nanoenergy and Nanosystems, Chinese Academy of Sciences, Beijing 101400, PR China

<sup>c</sup> School of Nanoscience and Technology, University of Chinese Academy of Sciences, Beijing 100049, PR China

<sup>d</sup> School of Materials Science and Engineering Georgia Institute of Technology, Atlanta, GA 30332-0245, USA

\* Corresponding author: Key Laboratory of Industrial Internet of Things and Networked Control, Ministry of Education, Chongqing University of Posts and Telecommunications, Chongqing, 400065, China

\*\* Corresponding author: Beijing Institute of Nanoenergy and Nanosystems, Chinese Academy of Sciences, Beijing 101400, PR China

E-mail addresses: gaosh@cqupt.edu.cn (S. Gao), zlwang@gatech.edu (Z.L. Wang)

<sup>1</sup> These authors contributed equally to this work

## Abstract

With the vigorous advancement of smart power grid, online monitoring is essential for a stable operation of overhead transmission lines. The energy supply that drives the monitoring system has become one of the bottlenecks restricting the development of distributed sensing systems. In view of the self-excited vibration with the characteristics of low-frequency and large-amplitude generated in the conductor galloping, a hybridized generator has been designed to be composed of an electromagnetic generator (EMG), a horizontal TENG (H-TENG), and a vertical TENG (V-TENG) to provide an alternative approach for capturing mechanical energy derived from conductor galloping. Based on triboelectric–electromagnetic working principal, a sophisticated-designed stator and rotor structure oriented to the application scenarios of transmission lines successfully achieved self-power through the designed EMG and galloping state sensing through the designed H-TENG and V-TENG, respectively. The output performance, feasibility and durability of the hybridized generator was well validated on the linear motor platform and the conductor galloping test platform, and the output current was used to realize the characterization of the conductor galloping amplitude and galloping trajectory. This work not only provides an effective and sustainable solution to the self-powered intelligent sensor nodes in the complex surroundings of power transmission system, but also reveals TENG promising potential on the sensing applications in low-power monitoring sensors for conductor galloping.

Keywords: Conductor galloping, Self-powered sensor, Hybridized generator, Galloping trajectory, Power transmission system

## 1. Introduction

Smart power grid plays an essential role in modern society<sup>[1]</sup>. Power transmission system is one of the most important parts of power grid. It mainly carries the

transmission of electric energy; potential defects or unforeseen failures within the power transmission system on power grids may lead to costly power outages and accidents<sup>[2,3]</sup>. Thus, online monitoring and fault diagnosis technology is necessary to ensure the safety and reliable transmission lines operation. The implementation of online monitoring of transmission lines depends on the development of sensor network with the limited energy distributed in a wide-complex region. These sensors can achieve the purpose of interconnection and human-computer interaction<sup>[4]</sup>. However, with a large increase in sensors, power supply has become a bottleneck, restricting the achievement of the long-term sensing requirements of transmission lines<sup>[5]</sup>. Traditional energy sources of sensors aimed at monitoring the condition of transmission lines including battery power supply, solar power and induction power supply. However, the problems of limited lifetime, environmental pollution, and low device maintainability have been exposed<sup>[6,7]</sup>, especially for the links in the power system that require real-time monitoring. Therefore, as a very promising alternative solution, environmental energy-harvesting technique can provide online monitoring system with powering. It can further utilize the energy resources in the surrounding environment of power transmission system, and a new and reliable self-powered sensor using green energy has become an extremely attractive solution.

Among the potential failures with the power transmission system, conductor galloping and aeolian vibration are one of the most serious faults in the operation of power transmission lines. Conductor galloping is a self-excited vibration phenomenon with low frequency (0.1–3 Hz) and large amplitude (5–300 times the diameter of the wire) induced by wind load and ice load on the transmission lines, and aeolian vibration is a wind excitation phenomenon with high frequency (3-150 Hz) and low amplitude<sup>[8-10]</sup>. Both of them cause fatigues, broken strands, even broken wires in transmission lines, seriously threatening the safety and reliability of power grid. It is noteworthy that, in severe cases due to the large amplitude, conductor galloping may bring power supply interruption and even hazards, such as flashover between line phase, strand breakage, and even tower collapse accidents<sup>[11, 12]</sup>. Therefore, online monitoring of transmission lines galloping is necessary to ensure the safety of

electricity. The vibration energy generated during the process of conductor galloping provides the feasibility for the application of self-powered sensors. Vibration energy-harvesting technique can be utilized given its advantages of harvesting and converting mechanical energy derived from conductor galloping into electric energy and self-powered sensing of conductor galloping degree. The electromagnetic generator (EMG) and triboelectric nanogenerator (TENG) are often used for vibration energy harvesting. Especially, TENG is not only a new energy technology, but also a very effective self-powered sensing technology. Thus far, TENG has been demonstrated to be the most effective approach to convert ambient mechanical energy into sustainable electrical energy<sup>[13-17]</sup> and realize high output performance. It can convert almost all types of mechanical power into electrical power<sup>[18-29]</sup>. TENG and EMG can be used as a complementary method due to the high output voltage of TENG and high output current of EMG<sup>[30-40]</sup>. In view of the irregular and multidirectional vibration motion of conductor galloping, an innovative idea that appropriately hybridizes the TENG and EMG is highly desired for the vibration energy harvesting induced by transmission lines galloping.

Here, a self-powered sensor to realize the self-powered sensing nodes of the power transmission system and sense the state and degree of conductor galloping based on the hybridized generator made of TENG and EMG is introduced. The unique design of TENG-EMG hybridized vibration energy harvester enables the system to collect the low-frequency vibration energy and irregular vibration efficiently induced by conductor galloping. To effectively monitor the degree of transmission lines galloping and harvest the vibration energy of different galloping state, we have designed the EMG, H-TENG, and V-TENG to monitor and harvest the galloping degree and vibration energy of horizontal and vertical direction. A linear motor platform with frequency, amplitude, and acceleration as variables was established to comprehensively evaluate the dynamic output of the module. It can verify the excellent output capability of the model and the ability to collect vibration energy with low frequency and large amplitude. Furthermore, the application scenarios of the scale reduction model of transmission lines galloping was built to verify the feasibility

and effectiveness of the model in terms of harvesting and sensing. This work provides a solution to the self-powered intelligent sensor nodes in the complex surroundings of the power transmission system.

## 2. Result and discussion

### 2.1 Structure and working principle

A self-powered and intelligent system consisting of magneto-electric and triboelectric hybridized generator was proposed for harvesting the vibration energy induced by power transmission lines galloping and monitoring the galloping state, as displayed in Fig. 1a. The designed TENG and EMG extract the vibration energy from the conductor galloping, especially the Horizontal-TENG (H-TENG) used for the energy harvesting and perception of horizontal vibration and Vertical-TENG (V-TENG) used for that of the vertical vibration, as displayed in Fig. 1b. Herein, H-TENG module is composed of stator and rotor. Design the structure and size can largely influence the characteristics of hybridized generator, including the number of blades and magnets on the rotor and coils on the stator. Structural optimization of hybridized generator was carried out to verify the output performance, as displayed in Figure S1 (Supporting Information), 6 blades and 3 magnets on the rotor and 5 coils on the stator was assembled in the hybridized generator. As shown in Figure S2c(Supporting Information), the stator is a hollow cylinder with a thickness of 5 mm and a radius of 85 mm made by 3D printing technology, the radius of the hollow part is 5 mm, and its surface has 12 fan rings that are evenly distributed. Twelve pieces of Cu electrodes are attached to the corresponding fan rings, and the copper electrodes are connected into two groups as the output terminal of energy. As shown in Figure S2d(Supporting Information), the rotor consists of three magnets, a bearing, and six fan ring blades evenly distributed around the bearing. The fan ring blade are made by 3D printing with a central angle of  $30^\circ$ , and the arched FEP films are pasted on the each fan ring blades. Three magnets are placed in the three blades, which are below the horizontal position of the bearing. As shown in Figure S2e(Supporting Information), the V-TENG module is composed of a stainless steel cuboid block, two

springs, a supporting fan ring, and two 3D printed boards that are attached together. Three pieces of FEP film are pasted on the stainless steel cuboid block. One end of the two springs is connected to the stainless steel cuboid block, and the other end is connected to the stainless steel supporting the fan ring. Six pieces of copper electrodes are distributed on the rectangular grooves from top to bottom, and six pieces of copper electrodes are connected to two groups as the energy output terminal. The EMG module is composed of five groups of coils on the 3D printed board and three pieces of magnets on the rotating fan ring blades. The coils are embedded in the cylindrical grooves of the two bonded 3D printed boards. In addition, to reduce the impact of the torsion and bending of the transmission line galloping on the model, an ABS tube is used to connect the stator and rotor, as well as the aluminum cable steel reinforced (ACSR) through the ABS tube.

The working principle of TENG with the example of a pair of electrodes is theoretically illustrated in Fig. 1c. The FEP film was assumed to be completely in contact with the electrode-1 at the initial state (Fig. 1c-i), and negative charges were generated on the FEP film through the triboelectrification; the same density of positive charges was generated on the electrode-1. When the blade moved toward electrode 2 (Fig. 1c ii-iv), which was induced by the external incentives, the positive charges in the loop were driven to move from electrode-1 to electrode-2 until the blade completely overlapped with electrode-2 (Fig. 1c v), at which point all positive charges moved to electrode-2, completing half a cycle. Then, the blade was driven to leave from electrode 2 and moved toward electrode-1 (Fig. 1c vi-viii) by the external incentives, forming a reverse current, until it overlapped with electrode-1 again (Fig. 1c i), completing the entire cycle. In addition, to further investigate the working principle of TENG, a finite element simulation of TENG was conducted using COMSOL software. The three-state potential distribution between FEP film and copper electrode was calculated and obtained, as depicted in Fig. 1d.

The generation mechanism of EMG based on electromagnetic induction with the example of a single coil is demonstrated in Fig. 1e. When the magnet rotated with the rotor, the magnetic flux passing through the coil would be changed. The coil was

assumed to be located between the three magnets at the initial state (Fig. 1e i), and no current was found in the coil. When the magnet moved away from the coil, the magnetic flux decreased and a clockwise current was generated in the coil to hinder the decline of the magnetic flux (Fig. 1e ii). When the magnet rotated to enable the coil to exceed the middle position of the two magnets, the magnetic flux through the coil began to increase, thereby generating a counterclockwise current in the coil (Fig. 1e iii). When the end of the magnet moved away from the coil, a clockwise current was generated again in the coil (Fig. 1e iv). The movement of the magnet is a reciprocating process, leading to the formation of a circulating current in the coil.

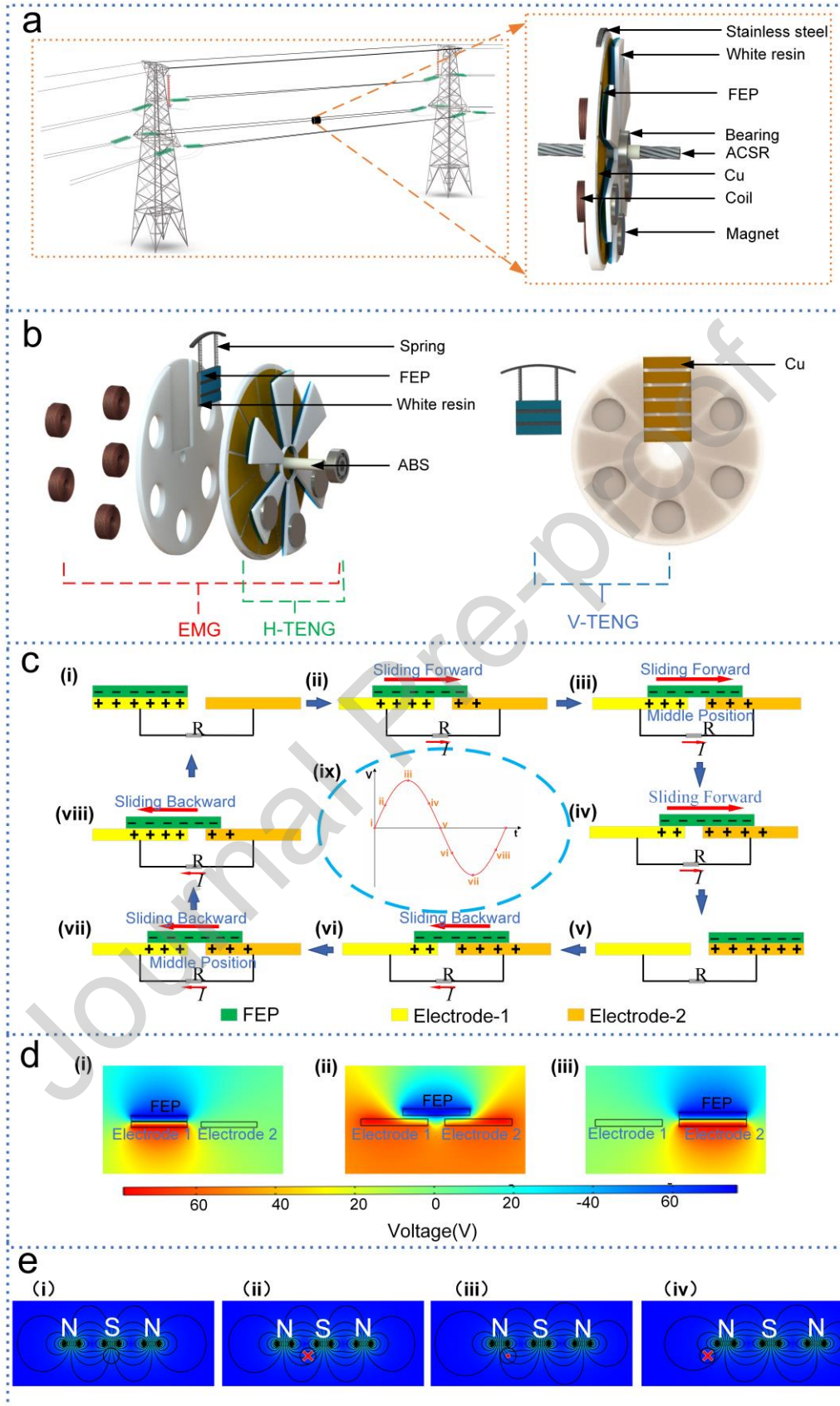


**Fig. 1.** Structure and working principle of the hybridized generator. a) Schematic illustrations of the generators and its application in the transmission lines galloping. b)

Detailed structure of the hybridized generator, including EMG, H-TENG, and V-TENG. c) Working principle of H-TENG and V-TENG. d) Electric potential distribution simulation of H-TENG and V-TENG by COMSOL. e) Magnetic field distribution simulation of EMG.

## 2.2 Output and characteristics of hybridized generator

To comprehensively evaluate the dynamic behavior of the hybridized generator oriented to the conductor galloping scenario, the performance of the hybridized generator was evaluated on a linear motor platform, and the effects of vibration frequency, vibration amplitude, and vibration acceleration on the output were systematically studied. In this work, aiming at the 4 mm diameter of aluminum clad steel wire (JL/G1A-25/4) used in the transmission line for voltage over 10 kV, four working strokes of the linear motor were selected to investigate the output characteristics of the hybridized generator oriented to the conductor galloping with the amplitude range of 5–30 cm (12.5–75 times of the wire diameter) under the frequency range of 0.7–2.8 Hz.

The influence of vibration frequency on the output of EMG under the condition of 5 cm stroke is displayed in Fig. 2a. The voltage and current peak value of EMG increased from 0.2 V to 1.02 V and 0.84 mA to 3.17 mA with the vibration frequency increasing from 0.7 Hz to 2.8 Hz. The output of EMG also exhibited a distinct uptrend with the increase in vibration frequency under the stroke conditions of 10, 20, and 30 cm, as depicted in Figure S3(Supporting Information). These results are consistent with the voltage and current output expression of EMG according to Faraday's law [41,42], as follows:

$$V_{EMG} = -N \frac{d\phi}{dt} \quad (1)$$

$$I_{EMG} = \frac{V_{EMG}}{R_{coil}} \quad (2)$$

where  $V_{EMG}$  represents the induced electromotive force generated in the coil,  $N$  represents the turn number of the coil,  $\phi$  represents the magnetic flux linkage of one turn coil, and  $t$  represents the time.  $R_{coil}$  and  $I_{EMG}$  represent the resistance of the coil

and the induced current, respectively. Thus, the increase in vibration frequency directly results in the increase in the change rate of the magnetic flux, further leading to the increase in the output voltage and current.

Then, the influence of the vibration amplitude on the output performance of EMG under different strokes at the vibration frequency of 1.2 Hz was investigated, as depicted in Fig. 2b. The voltage and current peak value of EMG increased from 0.28 V to 9.7 V and 0.93 mA to 15.87mA with the stroke increasing from 5 cm to 30 cm. This finding exhibits a directly increasing trend with increasing stroke. For the proposed EMG composed of a fixed coil and a movable magnet, according to Equation (1), the  $V_{EMG}$  can be further expressed as follows <sup>[43]</sup>:

$$V_{EMG} = -N \frac{d\phi}{dt} = -NS \frac{dB(x)}{dt} = -NS \frac{dB(x)}{dx} \frac{dx}{dt} = -NS \frac{dB(x)}{dx} v \quad (3)$$

where  $B(x)$  is the magnetic flux density through the coil,  $S$  is the area of the coil,  $x$  is the moving distance of the magnet, and  $v$  is the speed of the magnet. In addition, the horizontal speed component of the magnet is assumed to be always consistent with the speed of the linear motor, and the acceleration and deceleration processes were ignored when the linear motor changed the direction. Then, the speed of the linear motor can be expressed as follows:

$$v_{linear} = \frac{s}{t} \quad (4)$$

where  $s$  is the movement distance of the linear motor, and the speed of the magnet can be further expressed as follows:

$$v = \frac{v_{linear}}{\cos\theta} = \frac{s}{t \cos\theta} \quad (5)$$

where  $\theta$  is the angle between the magnet speed and the linear motor speed. Combining equations (2) and (4), the relation between voltage and stroke can be deduced, as follows:

$$V_{EMG} = -NS \frac{dB(x)}{dx} \frac{s}{t \cos\theta} \quad (6)$$

Therefore, the output voltage increased with the increase in the vibration stroke at the same magnet position. According to equation (2), the current also increased.

Finally, the influence of the different accelerations on the output performance of

EMG under the 10 cm stroke of the linear motor was investigated, as depicted in Fig. 2c. The output of EMG exhibited an evident uptrend with increasing acceleration from  $500 \text{ mm/s}^2$  to  $10000 \text{ mm/s}^2$ . While the acceleration was in the range of  $10000 \text{ mm/s}^2$  to  $30000 \text{ mm/s}^2$ , the output was almost unchanged due to the upper limitation of the rotation speed of the magnet under the current stroke condition. The increase in acceleration increased the speed of the rotor, thereby producing a greater rotation amplitude and change in magnetic flux under the condition of a fixed stroke; the output of EMG increased. However, the rotation speed of the magnet may reach its limit under the current stroke condition when the acceleration reached a certain value, and the output of EMG cannot continue to increase.

The designed EMG was tested on the linear motor to further verify its energy capture ability. The result showed that the EMG produced effective power supply effects under the conditions of 20 cm and higher strokes. The energy supply performance of EMG was obtained under the condition of 20 cm stroke and 1.7 Hz vibration frequency. The capacitor charging ability of the EMG was demonstrated by increasing the voltage of the  $1000 \mu\text{F}$  capacitor to 4 V within 10 s (Fig. 2d). The output of the EMG was measured with external loads from  $1 \Omega$  to  $50 \text{ k}\Omega$ , and EMG produced an instantaneous peak power of 16.4 mW at the matched resistance of  $380 \Omega$  (Fig. 2e). It satisfied the requirements for the working mode of MCU in the online monitoring system aimed at the conductor galloping. Finally, the actual power supply of the EMG was tested and verified. The results showed that 100 LED lights were lighted up (Fig. 2f and Movie S2). In addition, when an external rectifier bridge was connected with a  $1000 \mu\text{F}$  capacitor and a zener diode in parallel, the temperature and humidity sensor were proven to work effectively after the capacitor was charged to 3.5 V.

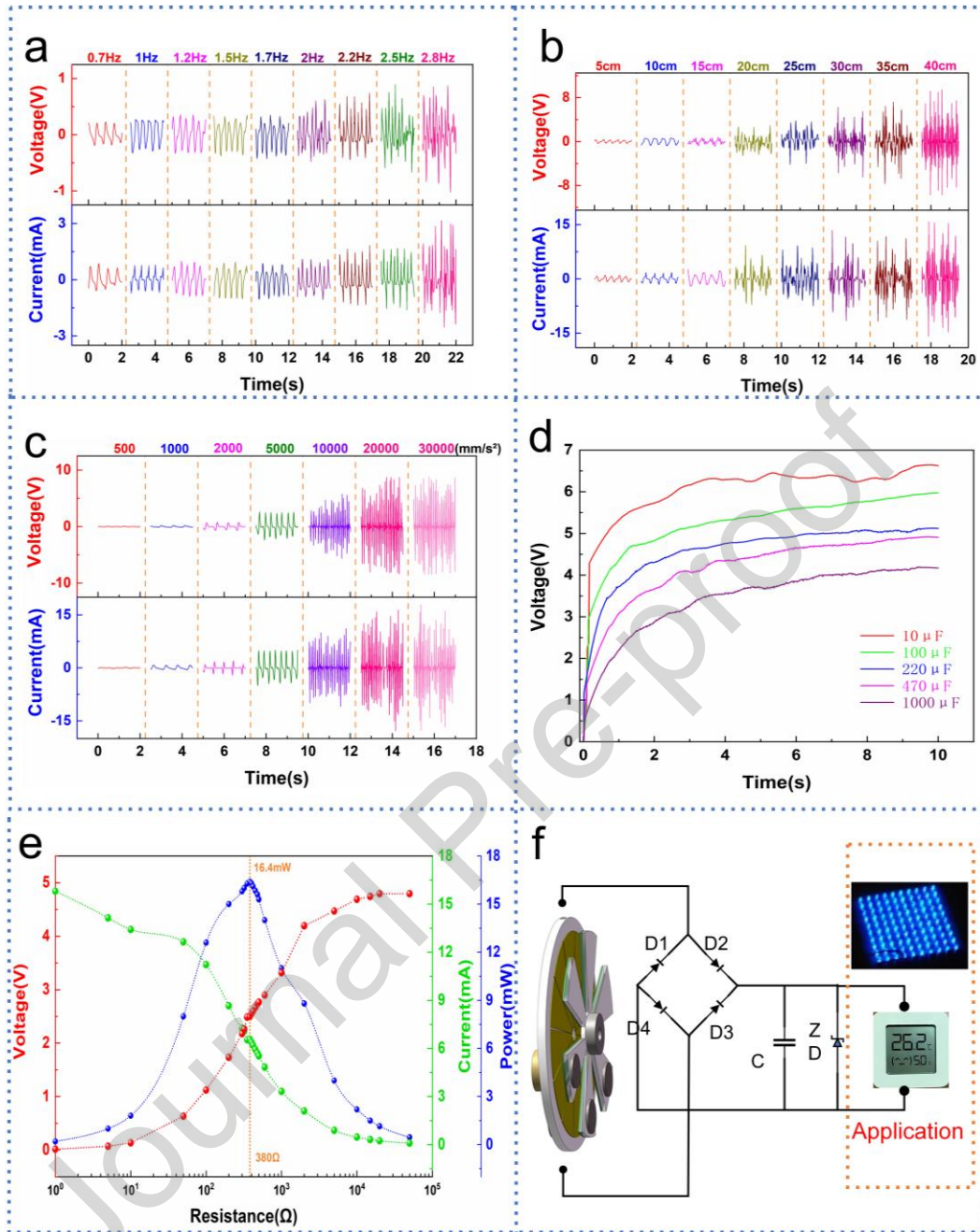


**Fig. 2.** Output performance of the hybridized generator on a linear motor. a) Output of the EMG in different frequencies. b) Output of the EMG in different strokes. c) Output of the EMG in different accelerations. d) Charge time of the EMG for different capacitors. e) Peak power with the external loading resistance (under the vibration stroke and frequency of 20 cm and 1.7 Hz). f) Supply energy to LED lights and temperature and humidity sensor.

For H-TENG and V-TENG, the effects of vibration frequency, vibration amplitude,

and vibration acceleration on the output were also systematically explored. The influence of vibration frequency on the output of H-TENG and V-TENG under the condition of 5 cm stroke is displayed in Fig. 3a and d, respectively. With the vibration frequency increasing from 0.7 Hz to 2.8 Hz, the voltage peak value of H-TENG and V-TENG increased from 3.86 V to 22.7 V and 1.44 V to 3.41 V. Moreover, the current peak value of H-TENG and V-TENG increased from 0.02  $\mu$ A to 0.52  $\mu$ A and 0.177  $\mu$ A, respectively, indicating that H-TENG has more potential performance of energy harvesting than V-TENG. In addition, under the stroke conditions of 10, 20, and 30 cm, the output of H-TENG and V-TENG exhibited a distinct uptrend with the increase in vibration frequency from 0.7 Hz to 1.5 Hz and 0.7 Hz to 2 Hz, respectively. However, when the vibration frequency of H-TENG and V-TENG reached 1.5 and 2 Hz, respectively, the voltage peak value of H-TENG and V-TENG remained 40 and 6 V, respectively, as displayed in Figure S4a-f (Supporting Information). The output voltage of TENG can be expressed as follows:

$$V_{TENG} = \frac{dQ}{dC} \quad (7)$$

where  $Q$  is the transfer charge between the TENG electrodes, and  $C$  is the equivalent capacitance of each TENG, which is only related to the material characteristics, shape, and size. For H-TENG, in view of the impact of the FEP film gravity, the film failed to make full contact with the copper electrode under the conditions of low frequency and low stroke. When the stroke and frequency reached a certain value, the FEP film was fully stretched and completely in contact with the stator electrode, and the charge reached saturation, resulting in almost constant voltage peak. The charge  $Q$  after reaching a stability can be expressed as follows:

$$Q = \frac{a}{180} \pi (r_2^2 - r_1^2) \sigma \quad (8)$$

where  $a$  is the center angle of copper electrode,  $r_2$  and  $r_1$  are the outer and inner radii of rotors, and  $\sigma$  is the equivalent triboelectric charge density. In addition, for V-TENG, under the conditions of low frequency and low stroke, only part of the FEP film on the stainless steel was in contact with the copper electrode. When the stroke and frequency reached a certain value, the FEP film was completely in contact with

the copper electrode during the vertical vibration process. The charge reached saturation, which can be expressed as follows:

$$Q = \sigma lw \quad (9)$$

where  $l$  and  $w$  are the length and width of the rectangular FEP film, respectively. Under the conditions of different strokes and accelerations, the voltage output of H-TENG and V-TENG also reached a stable peak value, as displayed in Fig. 3b–c and e–f.

However, the current output varied almost linearly with the increase in frequency, stroke, and acceleration, which was considered the core advantage of freestanding mode [40]. The current is the rate of charge transfer, which can be expressed as follows:

$$I = \frac{dQ}{dt} \quad (10)$$

As shown in Fig. 3a and d, the current output of H-TENG and V-TENG exhibited a direct uptrend with increasing frequency. The charge transfer rate increased with increasing frequency, resulting in the increase in the current output. For H-TENG, according to Equation (4), the increase in stroke in the same moving time accelerated the magnet's movement, resulting in a greater swing amplitude. Under the condition of the same frequency, the larger rotation amplitude leads to faster charge transfer between electrode 1 and electrode 2, eventually increasing the current output. For the V-TENG, under the conditions of the same frequency, the increase in stroke intensified the deformation degree of spring, resulting in more contact between the stainless steel block and copper electrodes during the reciprocating process. This condition leads to faster charge transfer between the electrodes and increase in current. In addition, the current variation of H-TENG was the same as that of EMG during the acceleration increased. As depicted in Fig. 3c, the output of H-TENG exhibited an evident uptrend with the acceleration increasing from  $500 \text{ mm/s}^2$  to  $20000 \text{ mm/s}^2$ . While the acceleration was in the range of  $20000 \text{ mm/s}^2$  to  $30000 \text{ mm/s}^2$ , the output was almost unchanged due to the upper limitation of the rotation speed. Thus, the charge transfer rate between electrode-1 and electrode-2 remained

unchanged. Similarly, the output of V-TENG exhibited an evident uptrend with increasing acceleration from  $500 \text{ mm/s}^2$  to  $10000 \text{ mm/s}^2$ . While the acceleration was in the range of  $10000 \text{ mm/s}^2$  to  $30000 \text{ mm/s}^2$ , the current output was basically unchanged, as displayed in Fig. 3f, because when the acceleration reached  $10000 \text{ mm/s}^2$ , the stainless steel block touched the bottom of the rectangular groove.

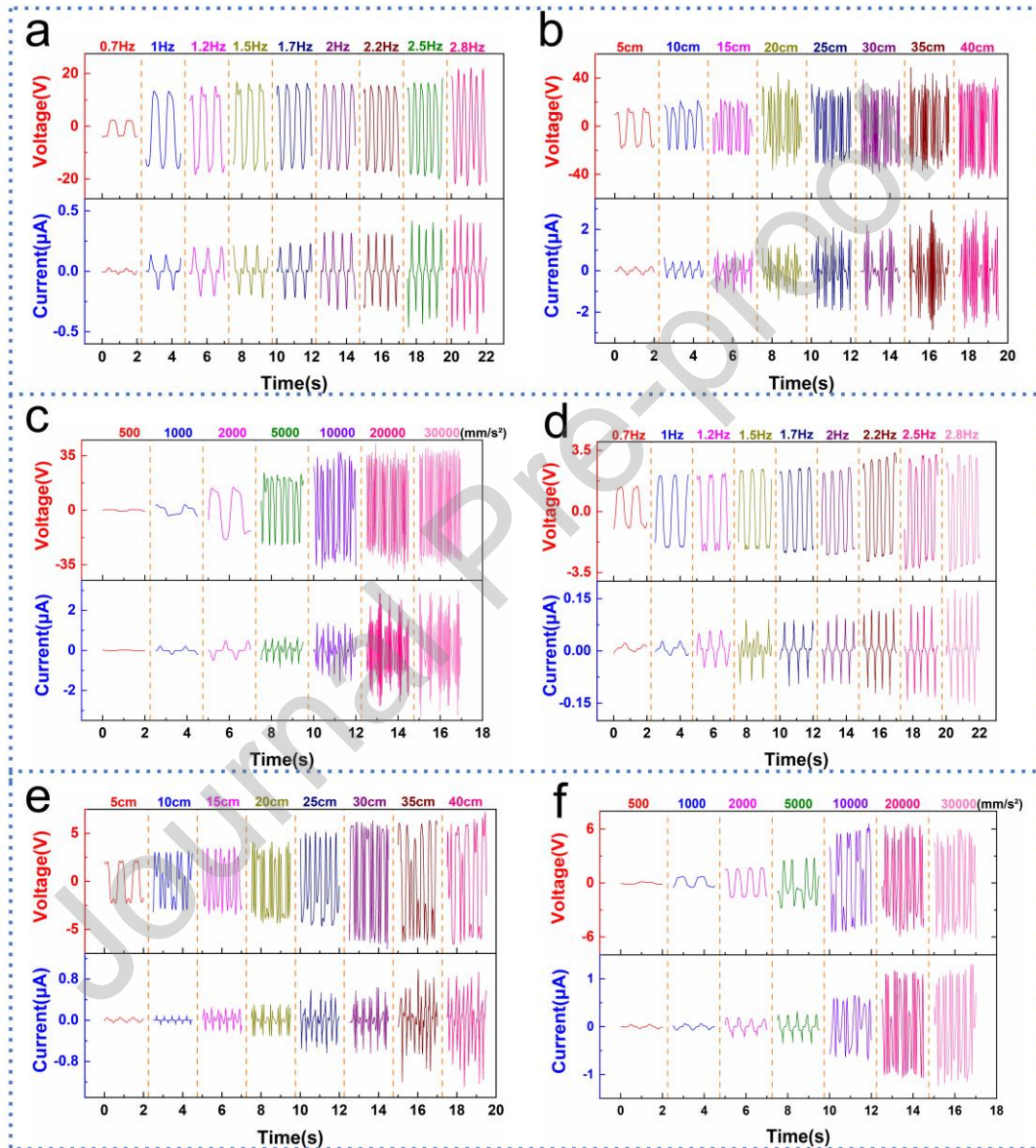


**Fig. 3.** a) Output of H-TENG in different frequencies. b) Output of H-TENG in different strokes. c) Output of H-TENG in different accelerations. d) Output of V-TENG in different frequencies. e) Output of V-TENG in different strokes. f) Output of V-TENG in different accelerations.

### 2.3 Hybridized generator's sensing ability for transmission lines galloping

A scaled reduction model of transmission lines galloping test platform was fabricated to illustrate the potential ability of the hybridized generator in the monitoring application of transmission lines galloping. It consists of a scaled reduction model of transmission line and a galloping testing machine, as depicted in Fig. 4a–d. The scaled reduction model of transmission line was made up of two supporting poles with a height of 1 m, two insulator strings and clamps, and an ACSR with a length of 3 m and a wire diameter of 6.98 mm, as depicted in Fig. 4c. The galloping testing machine based on three-degree-of-freedom reciprocating motor was fabricated to be composed of transverse reciprocating motor, longitudinal reciprocating motor, frequency and voltage regulator, as depicted in Fig. 4d. The longitudinal reciprocating motor was placed on the slide rail and connected with the transverse reciprocating motor to provide different vibration patterns through the cooperation with the transverse reciprocating motor, including horizontal vibration, vertical vibration, and approximate circular motion. It provided the different vibration types of the scaled-down transmission lines with adjustable amplitude of 0-15 cm and adjustable frequency of 0.7-2.8 Hz, effectively simulating the real conductor galloping state.

To verify the feasibility of the designed conductor galloping test platform, the galloping testing machine was used to provide different vibration patterns on the transmission line under the condition of 1.5 Hz vibration frequency, including horizontal vibration, vertical vibration, and approximate circular motion. An accelerated sensor was further used to measure the galloping amplitude driven by the galloping testing machine. The results showed that the transmission lines galloping test platform can effectively simulate the conductor galloping, which can be equivalent to a three-degree-of-freedom vibration, consisting of horizontal, vertical, and torsion. As a result, an irregular ellipse is obtained in the case of approximately circular motion from the point of view of motion trajectory. Among them, the maximum amplitude of the horizontal motion was 17 cm, the maximum amplitude of the vertical motion was 15 cm, the maximum amplitude of the long axis of the elliptic

motion was 11 cm, and the maximum amplitude of the short axis of the elliptic motion was 10 cm, as shown in Fig. 4e–g. The results exhibited that the amplitude of the conductor galloping in the horizontal motion was relatively larger than the vertical motion, indicating that the stroke in the horizontal direction was more conducive to energy harvesting of H-TENG and further providing a sensing solution for the conductor galloping based on the output performance of H-TENG and V-TENG. In summary, the designed galloping test platform can account for the scenario of transmission lines galloping to a certain extent.

Five working vibration conditions were selected to investigate the output performance of the EMG and H-TENG oriented to the horizontal motion, and the V-TENG oriented to the vertical motion of conductor galloping in the range of 0.7–2.2 Hz, respectively, as depicted in Fig. 4h–j. The figure shows that the output voltage of EMG, H-TENG, and V-TENG presented a directly increasing trend with the increase in vibration frequency; especially, the H-TENG exhibited a better output voltage. Then, the preliminary tests on the output of the composite generator in different galloping states at 1.5 Hz on the conductor galloping testing platform were conducted. The results indicated that H-TENG and V-TENG cannot harvest energy under the conditions of the single vertical motion and horizontal motion in the conductor galloping, respectively, as depicted in Fig. 4l and m. The transmission lines galloping prompted the rotation of the rotor of the EMG and H-TENG through bearing, which was mainly attributed to the contribution of the deflection of the rotor by the horizontal deflection force. Moreover, the amplitude in the horizontal direction affected the stroke of the rotor of EMG and H-TENG, directly determining the output performance. The single vertical force resulted in the slight torsion motion of transmission line, and the slight horizontal component also appeared. However, effectively prompting the rotation of the rotor of the EMG and H-TENG and producing power output are difficult. Analogously, V-TENG cannot harvest energy under the conditions of the single horizontal motion in the conductor galloping, as depicted in Fig. 4m, but it can harvest energy under the conditions of single vertical motion and elliptical galloping due to the impact of the vertical force on the vertical

vibration of the spring. Furthermore, in view of the appearance of torsion in the elliptical galloping state, the single horizontal and vertical galloping state had a larger stroke than the elliptical galloping state under the same vibration frequency. For the elliptical galloping state, the amplitude of the horizontal and vertical axis of the elliptical galloping induced by the galloping test machine was smaller than that of the single horizontal and vertical motion in the conductor galloping, respectively, as depicted in the Fig. 4e–g. Thus, the output of EMG and TENG under the conditions of elliptical galloping was smaller than that under the conditions of horizontal and vertical galloping.

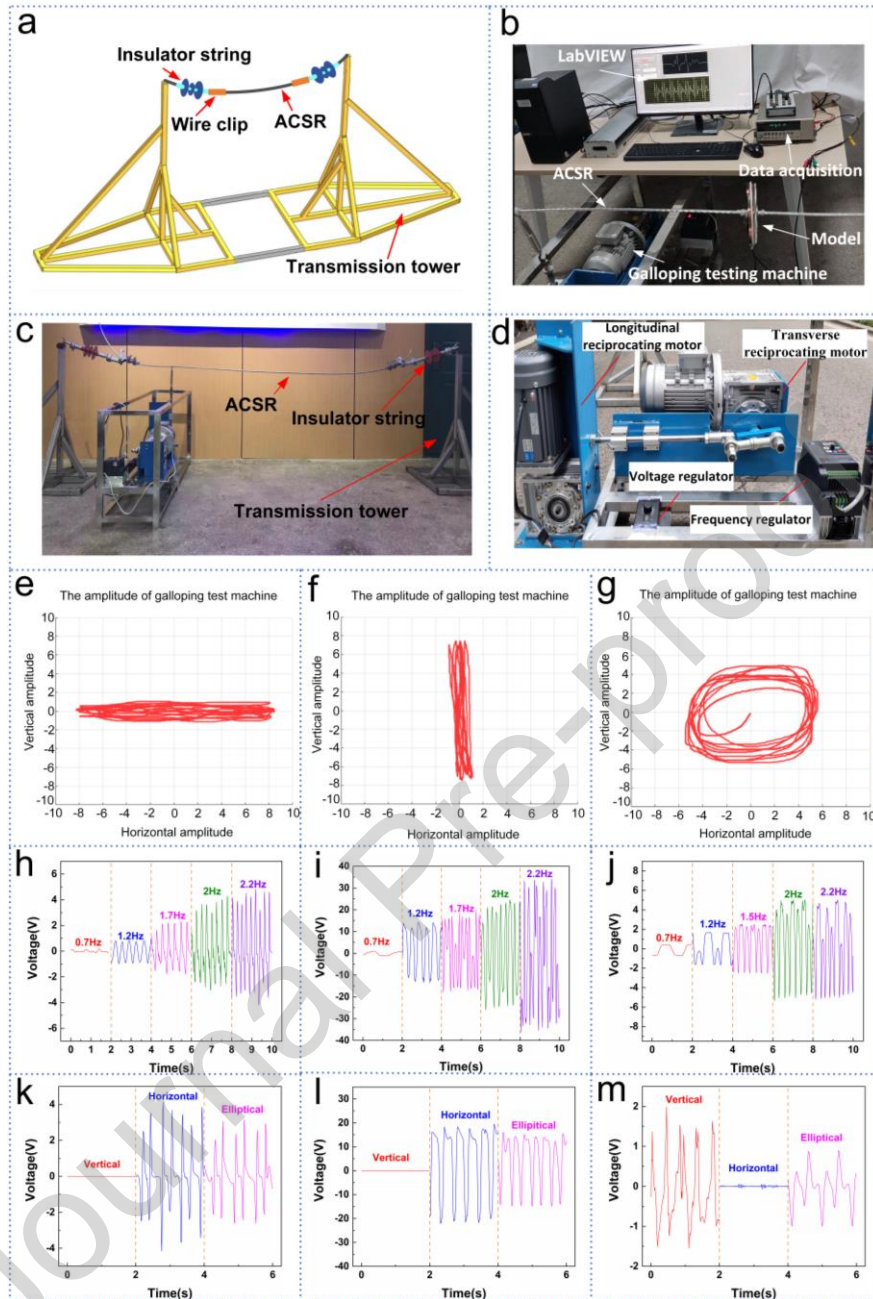


**Fig. 4.** Transmission lines galloping test platform and output of hybridized generator under the different galloping states. a) Scale reduction model of transmission line. b) Testing platform. c) Scale reduction model of transmission line galloping. d) Galloping testing machine. e) Amplitude in horizontal galloping state measured by the accelerated sensor. f) Amplitude in vertical galloping state measured by the accelerated sensor. g) Amplitude in elliptical galloping state measured by the accelerated sensor. h) Output of EMG in different frequencies. i) Output of H-TENG in different frequencies. j) Output of V-TRENG in different frequencies. k) Output of

EMG in different galloping states. l) Output of H-TENG in different galloping states.  
m) Output of V-TENG in different galloping states.

The monitoring of galloping amplitude is the key to achieve the long-term sensing needs of transmission lines galloping<sup>[44,45]</sup>. The output of the hybridized generator with different vibration amplitudes was further tested and investigated to verify the feasibility of the hybridized generator to achieve the monitoring of the transmission lines galloping state. For the conditions of horizontal galloping and elliptical galloping, the output of EMG exhibited a direct uptrend with the increasing vibration amplitude, as depicted in the Fig. 5a and b. Specifically, with the vibration amplitude of the horizontal galloping increased from 5.2 cm to 16.8 cm, the voltage peak value of EMG increased from 0.08 V to 5.55 V, and the current peak value increased from 0.81 mA to 10.65 mA. With the increase in the amplitude of the major axis of the elliptical galloping (horizontal direction) from 5 cm to 10.8 cm, the voltage peak value of EMG increased from 0.1 V to 5.68 V and 0.32 mA to 8.56 mA. The energy supply performance of EMG under the condition of elliptical galloping was better than that of horizontal galloping under the same horizontal amplitude. The torsion movement and vertical component motion triggered by the conductor vibration aggravated the motion displacement of the rotor of EMG and further promoted the output increasing. In addition, the voltage and current peak value of EMG reached 4 V and 7.8 mA, respectively, when the vibration amplitude (9.5 cm) of the elliptical galloping was about 18.3 times of the wire diameter (6.97 mm), and the output performance presented an uptrend with increasing stroke. This finding indicates that EMG can obtain effective output under the conditions of large-amplitude galloping. According to the previous results of load capacity of EMG based on the linear motor test, EMG had effective energy supply capacity to power the temperature and humidity sensor when the amplitude reached 20cm. Due to the design limitation of the galloping test machine, it cannot reach the vibration amplitude of EMG power supply output compared with the output based on linear motor platform, and the output of hybridized generator cannot reach the level of powering the temperature and humidity

sensor. However, it is noteworthy that the vibration amplitude of the HV transmissions lines galloping is much larger than the maximum amplitude induced from the galloping test machine. This finding exhibits that the EMG of the hybridized generator can provide effective energy supply for sensing system in the field of online monitoring actual application.

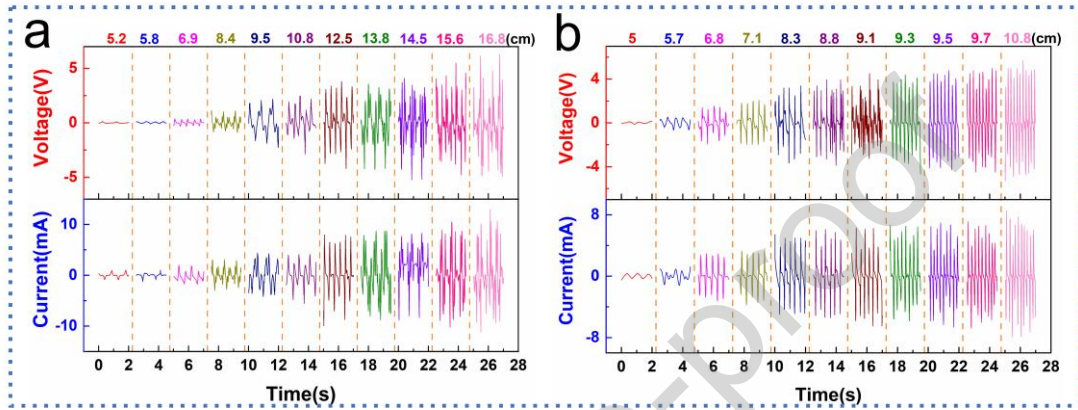


**Fig. 5.** Output of EMG on the galloping test machine. a) Output of EMG in the horizontal galloping state. b) Output of EMG in the elliptical galloping state.

The correlation between the output of the TENG and the vibration amplitude under the single direction excitation of the conductor galloping state was analyzed, and the average filtering peak detection circuit was used to obtain the peak value. For the H-TENG and V-TENG, the output characteristics had a significant positive correlation with the vibration amplitude of horizontal and vertical galloping, respectively. In addition, the increase in vibration amplitude further promoted the output performance. Specifically, with increasing vibration amplitude from 5.3 cm to 16.8 cm, the voltage and current peak value of H-TENG increased from 1.2 V to 40 V and 0.15  $\mu\text{A}$  to 2.8  $\mu\text{A}$ , respectively, as shown in Fig. 6a. With increasing vibration amplitude from 5.1 cm to 14.7 cm, the voltage and current peak value of V-TENG increased from 0.22 V to 5.91 V and 0.014  $\mu\text{A}$  to 0.77  $\mu\text{A}$ , respectively, as shown in Fig. 6c. Furthermore, when the vibration amplitude increased to 15.4 and 13.9 cm, the voltage of H-TENG and V-TENG remained stable, but the current continued to increase. The result indicated that the output current was more sensitive to the change in vibration amplitude, and the current peak value was linearly related to the amplitude variation

trend, as depicted in Fig. 6b and d. Finally, the correlation between the output of TENG and the vibration amplitude under the elliptical galloping state was further analyzed. Analogously, for H-TENG and V-TENG, the output characteristics had a significant positive correlation with the vibration amplitude of elliptical galloping. Specifically, with increasing vibration amplitude from 5 cm to 10.8 cm, the voltage and current peak value of H-TENG increased from 1.31 V to 28.9 V and 0.06  $\mu\text{A}$  to 0.82  $\mu\text{A}$ , respectively, as depicted in Fig. 6e. Furthermore, the voltage and current peak value of V-TENG exhibited a continuous rise with increasing amplitude, specifically from 0.29 V to 3.36 V and 0.01  $\mu\text{A}$  to 0.33  $\mu\text{A}$ , respectively, as depicted in Fig. 6g. The current peak value of H-TENG and V-TENG was also linearly related to the amplitude variation trend, as depicted in Fig. 6f and h. The figures show that the energy supply performance of H-TENG was superior to that of V-TENG, considering the different size and structure of the designed TENG. In summary, the peak value analysis, as a less energy consumption strategy, is the main analytical method, which can be used as a qualitative assessment to distinguish the contribution of horizontal and vertical components in the transmission lines galloping and the galloping degree on the premise of accumulating a large amount of measured data in future work. In addition, the output of each module in the hybridized generator can also be used as the basis for qualitative assessment of conductor galloping type. The hybridized generator was designed to be composed of H-TENG, V-TENG and EMG. The EMG and H-TENG of the hybridized generator produce output, while the little output of V-TENG indicates that the main occurrence of the horizontal galloping. On the contrary, the conductor only vibrates in the vertical galloping state when only V-TENG produces output. When EMG, H-TENG and V-TENG all produce output, the conductor vibrates in the elliptical galloping state.

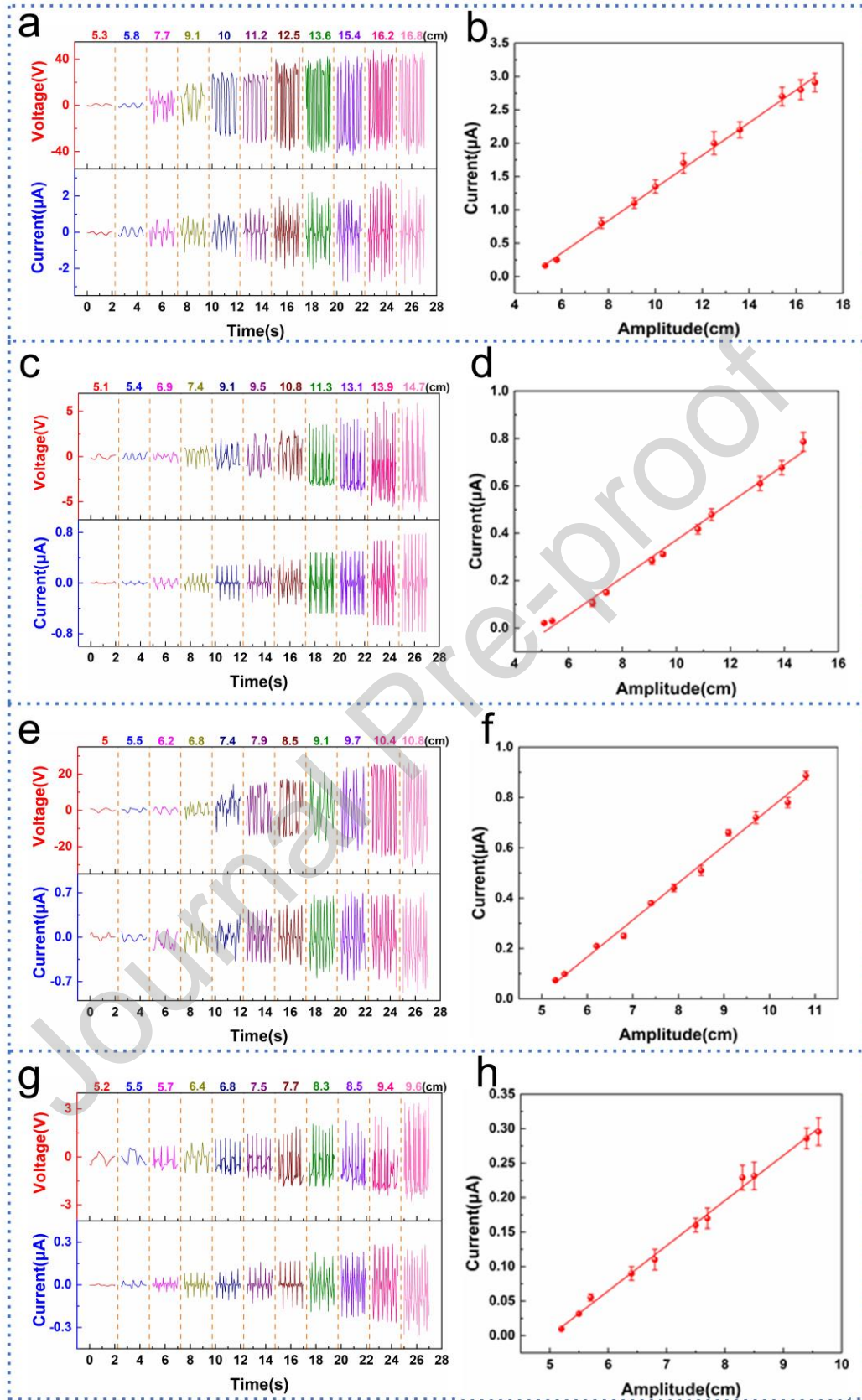


**Fig. 6.** Output of TENG on the galloping test machine and fit curve of amplitude. a) Output of H-TENG under horizontal galloping. b) Fit curve of amplitude under

horizontal galloping. c) Output of V-TENG under vertical galloping. d) Fit curve of amplitude under vertical galloping. e) Output of H-TENG under elliptical galloping. f) Fit curve of the major axis amplitude of elliptical galloping. g) Output of V-TENG under elliptical galloping. h) Fit curve of the minor axis amplitude of elliptical galloping.

In summary, the relationship between the galloping amplitude and the output current of TENG is linearly related to high goodness of fit. Specifically, the fitting relationship between the current of TENG and the vibration amplitude under the condition of different galloping patterns can be calculated and obtained, as shown in Table 1.  $x_h$  and  $x_v$  represent the horizontal and vertical displacements generated by the galloping test machine, respectively.  $i_h$  and  $i_v$  represent the output currents of H-TENG and V-TENG, respectively. The feasibility and reliability of the evaluation method of conductor galloping amplitude were further investigated through error analysis. The model of transmission line galloping testing platform was used to provide five different amplitudes  $x_a$  in each galloping state, which can be measured by the acceleration sensor. The output current of TENG under different galloping can be obtained by the hybridized generator, and the fitting galloping amplitude  $x$  can be calculated based on the above fitting formula. The relative error between  $x_a$  and  $x$  is defined as follows:

$$e = \frac{|x_a - x|}{x_a} \quad (11)$$

As shown in, Fig. 6b, d, f and h, the fitting galloping amplitudes were fairly close to the measured galloping amplitude. Specifically, the relative errors between the fitting galloping amplitude and the measured galloping amplitude under the condition of the single horizontal galloping, the single vertical galloping, and the elliptical galloping are 2.6%, 2.8%, 3.4% (major axis), and 4.2% (minor axis), respectively. The results indicate that the evaluation method of galloping amplitude provides a feasible solution for the perception of the conductor galloping state.

Table 1 Fitting equations between the galloping amplitude and output current of TENG

Different galloping patterns	Fitting formula	Goodness of fit
Single horizontal motion	$x_h = 4.10i_h + 4.54$	0.9974
Single vertical motion	$x_v = 12.54i_v + 5.33$	0.9958
Horizontal direction of elliptical motion	$x_h = 4.87i_h + 6.79$	0.9937
Vertical direction of elliptical motion	$x_v = 15.26i_v + 5.10$	0.9922

The feasibility of TENG in the field of monitoring of transmission lines galloping state was verified and explored combined with the galloping trajectory and fitting galloping amplitude. The characterization of the output of TENG on the galloping trajectory was further analyzed. In view of a certain periodicity of transmission lines galloping, the displacement in the vertical and horizontal directions can be approximated as a sinusoidal signal, and the interval time between two peaks is the galloping period  $T$ , as depicted in Figure S5 (Supporting Information). The trajectory output of one cycle measured by the acceleration sensor and the vibration amplitude calculated by the fitting formula were analyzed jointly, and the midpoint of the amplitude was calculated by the output current set at the origin, as depicted in Fig. 7d–f. The galloping trajectory had a small vertical and horizontal displacement in addition to the main direction displacement under the condition of single horizontal and vertical galloping, respectively, because the conductor galloping in a single direction caused the slight torsion movement, which triggered a slight movement in the other direction. In addition, the amplitude calculated by the output current of TENG according to the fitting formula had only horizontal or vertical direction because the designed H-TENG and V-TENG can only generate output in the horizontal and vertical vibration direction, not in the vertical and horizontal galloping state. On the contrary, the galloping trajectory had evident vertical and horizontal displacement under the condition of elliptical galloping, and the amplitude calculated by the output current of TENG had vertical and horizontal direction, reflecting the

major axis and minor axis of the elliptical galloping trajectory, respectively. In addition, the durability and stability of the designed hybridized generator is one of the most important performance indexes. Thus, the corresponding tests should be verify the durability and stability of the hybridized generator. For the single horizontal and elliptical galloping state, the hybridized generator was operated on the galloping test machine for 3 hours a day in 15 days under the vibration frequency of 1.2 Hz. The output voltage and current of the hybridized generator was tested every half an hour, and the average output of 3 hours was used for the output data of one day, as displayed in Figure S6 (Supporting Information). From the perspective of the continuous operation of 3 hours (Figure S6a-f) and 15 days (Figure S6g-i), the output fluctuation of the hybridized generator is less than 5.7% and 4.2%, respectively, indicating that the hybridized generator has good output stability and durability.

In summary, the evaluation method of conductor galloping amplitude based on the output current of TENG can reflect the galloping trajectory of the line to a certain extent, thereby providing a promising potential solution to effectively achieve the characterization of the galloping trajectory of the transmission line on the premise of accumulating a large amount of measured data in the further work. In the future, a sensing system for monitoring the conductor galloping state (Fig. 7g) can include the hybridized generator, distributed sensors, data acquisition terminals, and wireless communication modules, which can be an effective strategy to lay the foundation for the development and expansion of Power IoT. The TENG of the hybridized generator can obtain conductor galloping trajectory information in real time given the condition of insufficient power supply or outage maintenance of distributed sensors, and the EMG of the hybridized generator can achieve efficient conductor galloping energy collection for storage in supercapacitors and further provide power for a wireless unit to transmit data signal. Therefore, the design of a TENG-EMG generator offers a potential strategy for the fully self-powered and real-time monitoring conductor galloping state system by efficiently harvesting galloping energy.

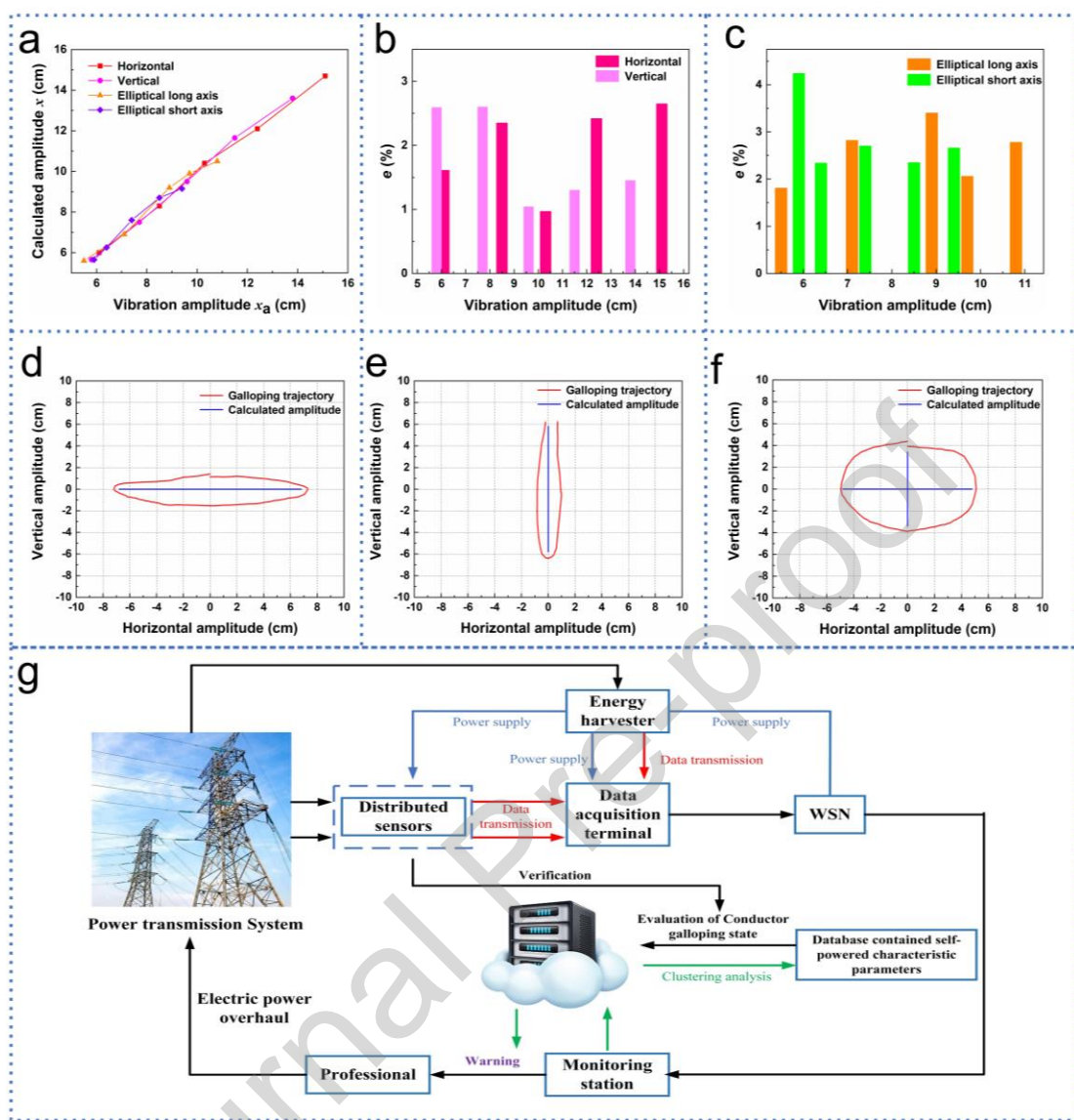


**Fig. 7.** Comparison analysis of the measured galloping trajectory and fitting galloping amplitude a) Amplitude comparison between  $x_a$  and  $x$ . b) Relative error of amplitude between  $x_a$  and  $x$  under the single direction galloping. c) Relative error of amplitude between  $x_a$  and  $x$  under the elliptical galloping. d) Comparison of the fitting galloping amplitude and measured galloping trajectory under the horizontal galloping. e) Comparison of the fitting galloping amplitude and measured galloping trajectory under the vertical galloping. f) Comparison of the fitting galloping amplitude and measured galloping trajectory under the elliptical galloping. g) Distributed sensor system for monitoring the conductor galloping state.

### 3. Conclusion

In summary, a hybridized generator based on triboelectric–electromagnetic has been designed to harvest the self-excited vibration energy of conductor galloping to supply power for the sensors of the power transmission system. Its joint utilization assesses the conductor galloping state. Through a sophisticated-designed hybridized generator of stator and rotor structure oriented to the application scenarios of transmission lines galloping, the vibration energy with the characteristics of low-frequency and large-amplitude is captured. On the linear motor platform, the impact of vibration frequency, vibration amplitude, and vibration acceleration on the hybridized generator were systematically investigated, effectively demonstrating the ability of the designed generator for vibration energy harvesting under the conditions of conductor galloping. Specially, EMG delivered a maximum power output of 16.4 mW (vibration frequency of 1.7 Hz and vibration amplitude of 20 cm), which is capable of satisfying the requirements for the working mode of low power MCU in the online monitoring system aimed at conductor galloping. In addition, H-TENG has more potential performance of energy harvesting than V-TENG under the designed size and structure. On the scaled reduction model of transmission lines galloping test platform, the output, feasibility and durability of the hybridized generator in the horizontal, vertical and elliptical galloping states was tested and analyzed. Due to the design limitation of the galloping test machine, it cannot reach the vibration amplitude of EMG power supply output compared with the output based on linear motor platform, but it is noteworthy that the vibration amplitude of the HV transmission lines galloping is much larger than the maximum amplitude induced from the galloping test machine. This finding exhibits that the EMG of the hybridized nanogenerator can provide effective energy supply for the sensing system in the field of online monitoring actual application. Finally, the output current of H-TENG and V-TENG can achieve a good linear fit to the amplitude of horizontal and vertical galloping and the amplitude of the horizontal long axis and the vertical minor axis in the elliptical galloping state, respectively. The galloping trajectory of the transmission line can be

characterized to a certain extent by the galloping amplitude obtained from the linear fitting results according to the output current of TENG. The peak value and trajectory analysis reveals the huge potential of TENG in the field of sensing the conductor galloping state.

#### 4. Experimental section

*Fabrication of the hybridized generator.* The hybridized generator was fabricated by 3D printed stator and rotor blade, magnets, coils, stainless steel blocks, and springs. The stator was produced by two laminated 3D printed white resin plates; one resin plate was designed as the 12 fan rings were evenly distributed on the surface. Twelve copper electrodes were pasted on the corresponding fan rings as the triboelectric electrodes. The rotor with six fan ring blades that were evenly distributed was produced by 3D printed blades and a bearing. The arched FEP film was attached on the ring blades as the triboelectric layer to form the H-TENG. A rectangular groove was fabricated on the surface of another resin plate in the stator, and the distance between the bottom of the groove and the stator center was designed as 6 mm. Six copper electrodes were pasted on one side of the rectangular groove as the triboelectric electrode. Three pieces of FEP film as the triboelectric layer were attached on the stainless steel block, which was connected to the spring and placed in the rectangular groove to form the V-TENG. Five cylindrical grooves were fabricated on the two laminated 3D printed boards with the distribution angle of 60. Five coils were embedded in the cylindrical grooves, and three cylindrical magnets were placed on the rotor blade to form the EMG. A hollow ABS cylinder passed through the stator and the bearing.

*Fabrication of the transmission lines galloping test platform.* The transmission lines galloping test platform included a scaled reduction model of transmission line and a galloping testing machine. The scale reduction model of the transmission line was fabricated as follows. Fxbw4-10/70 composite suspension insulator was used in the scaled model, one side of the insulator was fixed on the supporting pole, and the

other end was connected to the strain clamp. The aluminum conductor steel reinforced (ACSR) with an outer diameter of 6.97 mm was fixed and supported by strain clamp.

The galloping testing machine was composed of transverse and longitudinal reciprocating motors with compound operation; it was connected to the ACSR for galloping. The longitudinal reciprocating motor was placed on the slide rail and connected with the transverse reciprocating motor to provide different vibration patterns during the experiments. The transverse reciprocating motor generated a horizontal push–pull force to simulate the horizontal galloping state of the transmission line. The longitudinal reciprocating motor generated a vertical push–pull force to simulate the vertical galloping state of the transmission line, and the coordination work of the two motors was used to simulate the elliptical galloping state of the transmission line.

*Electrical measurement and characterization.* The output current and voltage of the hybridized generator were acquired by a programmable electrometer (Keithley 6514) and a Data Acquisition Card (NI PCI-6259) on a Desktop PC. The output data were excited by linear motor. The magnetic line of induction and TENG simulation were carried out with COMSOL Multiphysics 5.5.

#### **CRedit authorship contribution statement**

**Sihang Gao:** Conceptualization, Formal analysis, Funding acquisition, Methodology, Writing-original draft, Writing-review & editing. **Xisong Zeng:** Investigation, Modeling analysis, Experiment, Data curation, Writing-review & editing. **Guowen Zhang:** Investigation, Experiment, Supervision. **Jiajia Zhang:** Methodology, Validation. **Shaoxuan Feng:** Visualization, Experiment. **Yiduo Chen:** Supervision, Experiment. **Jie Zhou:** Experiment. **Wenyu Lan:** Experiment. **Zhong Lin Wang:** Conceptualization, Methodology, Supervision, Writing - review & editing. **Sihang Gao** and **Xisong Zeng** contributed equally to this work.

#### **Declaration of Competing Interest**

The authors declare that they have no known competing financial interests or personal relationships that could have appeared to influence the work reported in this paper.

## Acknowledgements

This work is supported and funded by The Scientific and Technological Research Program of Chongqing Municipal Education Commission of China (KJQN202000628) and the Fund Projects of the Natural Science Foundation of Chongqing Province of China (cstc2019jcyj-msxmX0070).

## Reference

- [1] F. X. Li, W. Qiao, H. B. Sun, H. Wan, J. H. Wang, Y. Xia, Z. Xu, P. Zhang, *IEEE Transactions on Smart Grid*, 17 (2010) 168-177. <https://doi.org/10.1109/TSG.2010.2053726>.
- [2] R. Morello, C. De Capua, G. Fulco, S. C. Mukhopadhyay, *IEEE Sensors Journal* 17 (2017) 7828-7837. <https://doi.org/10.1109/JSEN.2017.2760014>.
- [3] P. Akaber, B. Moussa, M. Ghafouri, R. Atallah, B. L. Agba, C. Assi, M. Debbabi, *IEEE Transactions on Smart Grid* 11 (2020) 2676-2687. <https://doi.org/10.1109/TSG.2019.2959937>.
- [4] R. Morello, S. C. Mukhopadhyay, Z. Liu, D. Slomovitz and S. R. Samantaray, *IEEE Sensors Journal* 17 (2017) 7596-7610. <https://doi.org/10.1109/JSEN.2017.2735539>.
- [5] J. Han, J. Hu, Y. Yang, Z. Wang, S. X. Wang, J. He, *IEEE Transactions on Industrial Electronics* 62 (2015) 4398-4407. <https://doi.org/10.1109/TIE.2014.2383992>.
- [6] Z. J. Chew, T. Ruan, M. Zhu, *IEEE Trans. on Power Electronics* 34 (2019) 8671-8681. <https://doi.org/10.1109/TPEL.2018.2885827>.
- [7] M. K. Stojcev, M. R. Kosanovic, L. R. Golubovic, 9th Int. Conf. on Telecommunication in Modern Statellite, Cable, and Broadcasting Services, 2009, pp.65-72. <https://doi.org/10.1109/TELSKS.2009.5339410>.
- [8] A. T. Edwards, A. Madeyski, *Transactions of the American Institute of Electrical Engineers. Part III: Power Apparatus and Systems* 75 (1956) 666-686. <https://doi.org/10.1109/AIEEPAS.1956.4499353>.
- [9] J. W. Wang, J. L. Lilien, *IEEE Transactions on Power Delivery* 13 (1998) 909-916. <https://doi.org/10.1109/61.686992>.
- [10] J. L. Lilien, D. G. Havard, *IEEE Transactions on Power Delivery* 15 (2000) 670-674. <https://doi.org/10.1109/61.853003>.
- [11] M. Farzaneh, *Phil. Trans. R. Soc. A.* 358 (2000) 2971-3005. <https://doi.org/10.1098/rsta.2000.0692>.
- [12] O. Nigol, P. G. Buchan, *IEEE Trans. Power App. Syst.* PAS-100 (1981) 699-707. <https://doi.org/10.1109/TPAS.1981.316921>.

- [13] H. Guo, J. Chen, L. Tian, Q. Leng, Y. Xi, C. Hu, *ACS Appl. Mater. Interfaces* 6 (2014) 17184-17189.  
<https://doi.org/10.1021/am504919w>.
- [14] J. Wang, C. Wu, Y. Dai, Z. Zhao, A. Wang, T. Zhang, Z. L. Wang, *Nat. Commun.* 8 (2017) 88.  
<https://doi.org/10.1038/s41467-017-00131-4>.
- [15] L. Xu, T. Jiang, P. Lin, J. J. Shao, C. He, W. Zhong, X. Y. Chen, Z. L. Wang, *ACS Nano* 12 (2018) 1849-1858.  
<https://doi.org/10.1021/acsnano.7b08674>.
- [16] D. Anaya, T. He, C. Lee, M. Yuce, *Nano Energy* 72 (2020) 104675.  
<https://doi.org/10.1016/j.nanoen.2020.104675>.
- [17] C. Qiu, F. Wu, C. Lee, M. Yuce, *Nano Energy* 70 (2020) 104456.  
<https://doi.org/10.1016/j.nanoen.2020.104456>.
- [18] M. Xu, P. Wang, Y. C. Wang, S. L. Zhang, A. C. Wang, C. Zhang, Z. Wang, X. Pan, Z. L. Wang, *Adv. Energy Mater.* 8 (2018) 1702432. <https://doi.org/10.1002/aenm.201702432>.
- [19] S. Gao, M. Wang, Y. Chen, M. Tian, Y. Zhu, X. Wei, T. Jiang, *Nano Energy* 45 (2018) 21-27.  
<https://doi.org/10.1016/j.nanoen.2017.12.021>.
- [20] G. Zhu, J. Chen, T. Zhang, Q. Jing, Z. L. Wang, *Nat. Commun.* 5 (2014) 3426.  
<https://doi.org/10.1038/ncomms4426>.
- [21] X. Wang, S. Wang, Y. Yang, Z. L. Wang, *ACS Nano* 9 (2015) 4553-4562.  
<https://doi.org/10.1021/acsnano.5b01187>.
- [22] S. X. Li, D. Liu, Z. H. Zhao, L. L. Zhou, X. Yin, X. Y. Li, Y. K. Gao, C. G. Zhang, Q. Zhang, J. Wang, Z. L. Wang, *ACS Nano* 14 (2020) 2475-2482. <https://doi.org/10.1021/acsnano.9b10142>.
- [23] S. Gao, Y. Chen, J. Su, M. Wang, X. Wei, T. Jiang, Z. L. Wang, *ACS Nano* 11 (2017) 3965-3972.  
<https://doi.org/10.1021/acsnano.7b00422>.
- [24] M. Xu, Y. C. Wang, S. L. Zhang, W. Ding, J. Cheng, X. He, P. Zhang, Z. Wang, X. Pan, Z. L. Wang, *Extreme Mech. Lett.* 15 (2017) 122-129. <https://doi.org/10.1016/j.eml.2017.07.005>.
- [25] R. Liu, X. Kuang, J. Deng, Y. C. Wang, A. C. Wang, W. Ding, Y. C. Lai, J. Chen, P. Wang, Z. Lin, H. J. Qi, B. Sun, Z. L. Wang, *Adv. Mater.* 30 (2018) 1705195. <https://doi.org/10.1002/adma.201705195>.
- [26] S. Gao, J. Su, X. Wei, M. Wang, M. Tian, T. Jiang, Z. L. Wang, *ACS Nano* 11 (2017) 770-778.  
<https://doi.org/10.1021/acsnano.6b07183>.
- [27] L. Pan, J. Wang, P. Wang, R. Gao, Y. C. Wang, X. Zhang, J. J. Zou, Z. L. Wang, *Nano Res.* 11 (2018) 4062-4073. <https://doi.org/10.1007/s12274-018-1989-9>.

- [28] S. L. Zhang, M. Xu, C. Zhang, Y. C. Wang, H. Zou, X. He, Z. Wang, Z. L. Wang, *Nano Energy* 48 (2018) 421-429. <https://doi.org/10.1016/j.nanoen.2018.03.062>.
- [29] X. Wang, Z. L. Wang, Y. Yang, *Nano Energy* 26 (2016) 164-171.  
<https://doi.org/10.1016/j.nanoen.2016.05.032>.
- [30] L.X. Gao, X. Chen, S. Lu, H. Zhou, W.B. Xie, J.F. Chen, M.K. Qi, H. Yu, X.J. Mu, Z.L. Wang, Y. Yang, *Adv. Energy Mater.* 10 (2019) 1902725. <https://doi.org/10.1002/aenm.201902725>.
- [31] S. Wang, X. Mu, Y. Yang, C. Sun, A. Gu, Z. L. Wang, *Adv. Mater.* 27 (2015) 240–248.  
<https://doi.org/10.1002/adma.201403944>.
- [32] Y. Zi, H. Guo, Z. Wen, M. Yeh, C. Hu, Z. L. Wang, *ACS Nano* 10 (2016) 4797-4805.  
<https://doi.org/10.1021/acsnano.6b01569>.
- [33] E. Koukharenko, S. Beeby, M. Tudor, N. White, T. Donnell, C. Saha, S. Kulkarni, S. Roy, *Microsyst. Technol.* 12 (2006) 1071–1077. <https://doi.org/10.1007/s00542-006-0137-8>.
- [34] P. Wang, R. Liu, W. Ding, P. Zhang, L. Pan, G. Dai, H. Zou, K. Dong, C. Xu, Z. L. Wang, *Adv. Funct. Mater.* 28 (2018) 1705808. <https://doi.org/10.1002/adfm.201705808>.
- [35] C. Zhang, W. Tang, C. Han, F. R. Fan, Z. L. Wang, *Adv. Mater.* 26 (2014) 3580-3591.  
<https://doi.org/10.1002/adma.201400207>.
- [36] Z. Y. Wu, B. B. Zhang, H. Y. Zou, Z. M. Lin, G. L. Liu, Z. L. Wang, *Adv. Energy Mater.* 9(2019) 1901124.  
<https://doi.org/10.1002/aenm.201901124>.
- [37] X. Q. Zhang, M. Yu, Z. R. Ma, H. Ouyang, Y. Zou, S. L. Zhang, H. K. Niu, X. X. Pan, M. Y. Xu, Z. Li, Z. L. Wang, *Adv. Funct. Mater.* 29 (2019) 1900327. <https://doi.org/10.1002/adfm.201900327>.
- [38] J. B. Yu, X. J. Hou, M. Cui, S. N. Zhang, J. He, W. P. Geng, J. L. Mu, X. J. Chou, *Nano Energy* 64 (2019) 103923. <https://doi.org/10.1016/j.nanoen.2019.103923>.
- [39] F. F. Sheng, J. Yi, S. Shen, R. W. Cheng, C. Ning, L. Y. Ma, X. Peng, W. Deng, K. Dong, Z. L. Wang, *ACS Appl. Mater. Interfaces* 13 (2021) 44868-44877. <https://doi.org/10.1021/acsami.1c12378>.
- [40] S. Yong, J.Y. Wang, L. J. Yang, H. Q. Wang, H. Luo, R. J. Liao, Z. L. Wang, *Adv. Energy Mater.* 11 (2021) 2101194. <https://doi.org/10.1002/aenm.202101194>.
- [41] P. Wang, R. Liu, W. Ding, P. Zhang, L. Pan, G. Dai, H. Zou, K. Dong, C. Xu, Z. L. Wang, *Adv. Funct. Mater.* 28 (2018) 1705808. <https://doi.org/10.1002/adfm.201705808>.
- [42] H. Guo, Z. Wen, Y. Zi, M. Yeh, J. Wang, L. Zhu, C. Hu, Z. L. Wang, *Adv. Energy Mater.* 6 (2016) 1501593.  
<https://doi.org/10.1002/aenm.201501593>.

- [43] L. X. Gao, S. Lu, W. B. Xie, X. Chen, L. K. Wu, T. T. Wang, A. B. Wang, C. Q. Yue, D. Q. Tong, W. Q. Lei, H. Yu, X. B. He, X. J. Mu, Z. L. Wang, Y. Yang, *Nano Energy* 72 (2020) 104684.  
<https://doi.org/10.1016/j.nanoen.2020.104684>.
- [44] Z. Ding, X. Zhang, N. Zou, F. Xiong, Y. Zhang, *Journal of Lightwave Technology* 39 (2021) 5163-5169.  
<https://doi.org/10.1109/JLT.2021.3078747>.
- [45] H. Zou, M. Lu, *IEEE Access* 9 (2021) 30893-30897. <https://doi.org/10.1109/ACCESS.2021.3055820>.

#### Biographies



**Sihang Gao** received his Ph.D. degree in electrical engineering from Chongqing University, China in 2017. He is currently associate professor in Chongqing University of Posts and Telecommunications. His research interests are mainly focused on theoretical studies of triboelectric nanogenerators, and practical applications of energy harvesting and sensing in power grid environment.



**Xisong Zeng** is currently postgraduate student of Chongqing University of Posts and Telecommunications. His research interests are mainly focused on self-powered sensing systems based on triboelectric nanogenerators, and practical applications in vibration energy harvesting.



**Guowen Zhang** was a postgraduate student of Chongqing University of Posts and Telecommunications. His research interests are mainly focused on vibration energy harvesting and self-powered systems.



**Jiajia Zhang** received his Ph.D. degree in measurement and control technology and instrumentation from Chongqing University, China in 2015. He is currently lecturer in Chongqing University of Posts and Telecommunications. His research interests are mainly focused on Self-powered sensing technology, and practical applications of energy harvesting.



**Yiduo Chen** is currently postgraduate Student of Chongqing University of Posts and Telecommunications. His research interests are mainly focused on self-powered sensing systems based on triboelectric nanogenerators, and practical applications in blue energy harvesting.



**Shaoxuan Feng** is currently postgraduate Student of Chongqing University of Posts and Telecommunications. His research interests are mainly focused on paper-based flexible electronic devices, and practical applications in flexible perception.



**Wenyu Lan** is currently undergraduate Student of Chongqing University of Posts and Telecommunications. His research interest is self-powered sensing systems based on triboelectric nanogenerators.



**Jie Zhou** is currently undergraduate Student of Chongqing University of Posts and Telecommunications. His research interest is self-powered sensing systems based on triboelectric nanogenerators.



**Prof. Zhong Lin Wang** received his Ph.D. degree from Arizona State University in physics. He now is the Hightower Chair in Materials Science and Engineering, Regents' Professor at Georgia Tech, the chief scientist and director of the Beijing Institute of Nanoenergy and Nanosystems, Chinese Academy of Sciences. Prof. Wang has made original and innovative contributions to the synthesis, discovery, characterization and understanding of fundamental physical properties of oxide nanobelts and nanowires, as well as applications of nanowires in energy sciences, electronics, optoelectronics and biological science. His discovery and breakthroughs in developing nanogenerators establish the principle and technological road map for harvesting mechanical energy from environmental and biological systems for powering personal electronics. His research on self-powered nanosystems has inspired the worldwide efforts in academia and industry for studying energy for micro-nano-systems, which is now a distinct disciplinary in energy research and future sensor networks. He coined and pioneered the fields of piezotronics and piezophotonics by introducing piezoelectric potential gated charge transport process in fabricating new electronic and optoelectronic devices.

#### **CRedit authorship contribution statement**

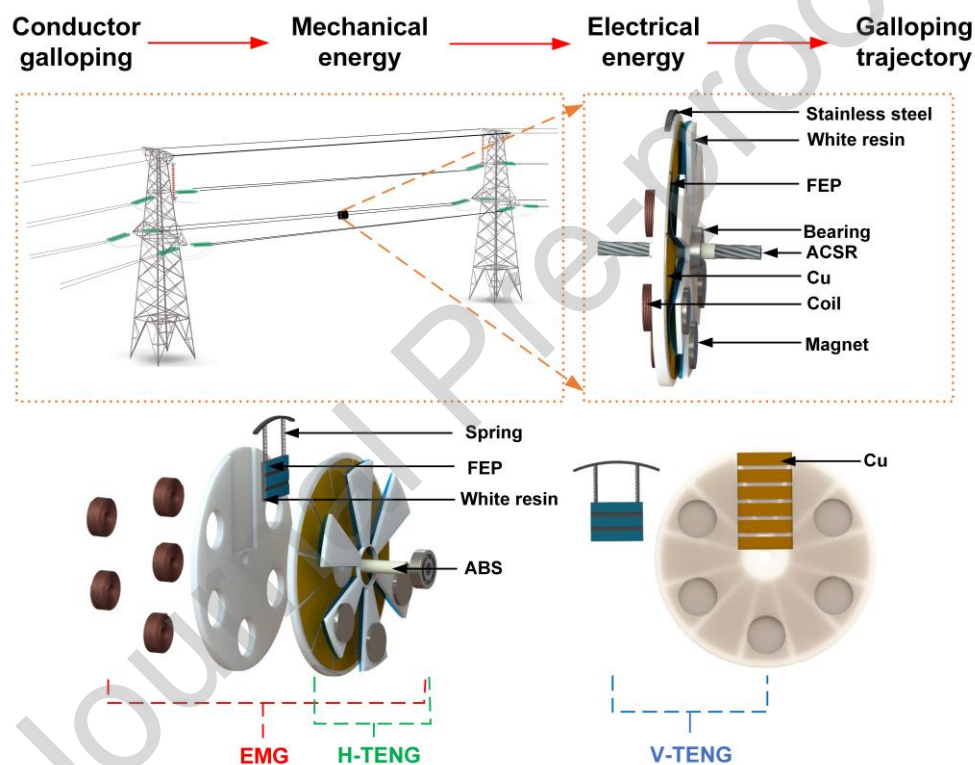
**Sihang Gao**: Conceptualization, Formal analysis, Funding acquisition, Methodology, Writing-original draft, Writing-review & editing. **Xisong Zeng**: Investigation, Modeling analysis, Experiment, Data curation, Writing-review & editing. **Guowen Zhang**: Investigation, Experiment, Supervision. **Jiajia Zhang**: Methodology, Validation. **Shaoxuan Feng**: Visualization, Experiment.

**Yiduo Chen:** Supervision, Experiment. **Jie Zhou:** Experiment. **Wenyu Lan:** Experiment. **Zhong Lin Wang:** Conceptualization, Methodology, Supervision, Writing - review & editing. **Sihang Gao** and **Xisong Zeng** contributed equally to this work.

### Declaration of Competing Interest

The authors declare that they have no known competing financial interests or personal relationships that could have appeared to influence the work reported in this paper.

## Graphical Abstract



## Highlights

- This work is characterized by the first propose of harvest the energy of conductor galloping by converting mechanical energy to electrical energy and the joint utilization thereof to assessment the galloping trajectory.
- Through a sophisticated-designed hybridized generator of stator and rotor structure oriented to the application scenarios of transmission lines, the vibration energy with the characteristics of low-frequency and large-amplitude is captures.
- The peak value and trajectory analysis reveals the huge potential of TENG in the field of sensing the conductor galloping state.

Journal Pre-proof